ACS APPLIED MATERIALS & INTERFACES

Research Article

www.acsami.org

Supercritical CO_2 Mediated Incorporation of Pd onto Templated Carbons: A Route to Optimizing the Pd Particle Size and Hydrogen Uptake Density

Eric Masika, Richard A. Bourne, Thomas W. Chamberlain, and Robert Mokaya*

University of Nottingham, University Park, Nottingham NG7 2RD, U.K.

Supporting Information

ABSTRACT: Palladium nanoparticles are deposited onto zeolite template carbon (ZTC) via supercritical CO_2 ($scCO_2$) mediated hydrogenation of a CO_2-phillic transition metal precursor. The supercritical fluid (SCF) mediated metal incorporation approach enabled the decoration of ZTC with 0.2−2.0 wt % of well-dispersed Pd nanoparticles of size 2−5 nm. The resulting Pd-doped ZTCs exhibit enhanced hydrogen uptake and storage density. The ZTC (with surface area of 2046 m^2/g) had a hydrogen storage capacity (at 77 K and 20 bar) of 4.9 wt %, while the Pd-ZTCs had uptake of 4.7−5.3 wt % despite a surface area in the range 1390−1858 m^2/g. The Pd-ZTCs thus exhibit enhanced hydrogen storage density (14.3−18.3 μmol H_2/m^2), which is much higher than that of Pd-free ZTC (12.0 μmol H_2/m^2). The hydrogen isosteric heat of adsorption (Q_{st}) was found to be higher for the Pd-doped carbons (6.7 kJ/mol) compared to the parent ZTC (5.3 kJ/mol). The deposition of small amounts of Pd (up to 2 wt %) along with well-dispersed Pd nanoparticles of size of 2−5 nm is essential for the enhancement of hydrogen uptake and illustrates the importance of optimizing the balance between metal loading/particle size and surface area to achieve the best metal/porous carbon composite for enhanced hydrogen uptake.

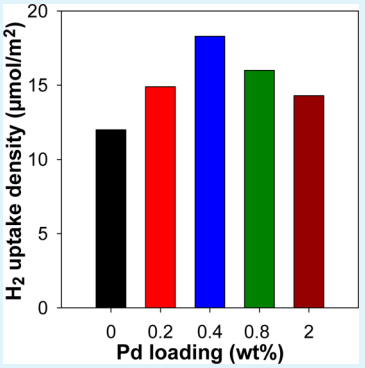

KEYWORDS: *hydrogen storage, zeolite-templated carbon, palladium nanoparticles, supercritical CO_2, pore size distribution*

1. INTRODUCTION

Porous carbons, due to their tunable porosity and surface functionality coupled with their existence in a variety of forms (powders, fibers, forms, composites, among others), are potentially useful hydrogen storage materials.[1,2] Carbonaceous nanostructured materials have very unique surface textures and porosities that can be readily modulated to give high surface area and well-ordered pore systems. Highly porous carbons may be prepared via a number of synthesis procedures including activation (physical and chemical)[3−8] or template carbonization.[9−20] In the template carbonization methodology, an inorganic porous template characterized by a unique nanospace such as a zeolite matrix is used to define the porosity of the carbon. The advantage of using materials with well-defined texture and pore size distribution for hydrogen storage lies in the possibility of relating the hydrogen uptake properties to the textural properties of the adsorbent. In recent years, intensive research on the use of porous carbon materials as hydrogen stores has established a correlation between surface area (associated with microporosity) and hydrogen storage.[18−27] In addition, some studies have proposed that micropores between 0.6 and 0.8 nm are the most efficient for hydrogen storage.[23,24,26−28]

On the other hand, it has been suggested that dispersed metal nanoparticles within a high surface area substrate (such as a porous carbon) can enhance hydrogen storage. It is thought that the resulting metal/porous material composites may take up hydrogen via two processes: (i) adsorption of hydrogen on the surface of the pores of the porous material and (ii) hydrogenation on the metal nanoparticles by forming metal hydrides.[29] The latter process (hydrogenation) is due to chemisorption of atomic hydrogen on the metal nanoparticles, which can then initiate a mechanism referred to as hydrogen "spillover".[30−33] Furthermore, Nalm and co-workers have established that hydrogen spillover does not only improve hydrogen capacity but also increases initial hydrogen adsorption kinetics.[34] However, the very existence of a spillover mechanism has been strongly debated with some experimental results reporting findings that revealed very low hydrogen capacities after metal doping.[35,36] The details of spillover as applied in hydrogen storage processes are thus yet to be clearly understood due to the disparity in experimental data.[37−40] Nevertheless, the spillover of atomic hydrogen is a well-established process in heterogeneous catalysis.[37−40]

The synthesis of metal nanoparticles and subsequent dispersion into high surface area carbons can be carried out by either chemical or physical methods, including wet impregnation,[30,41] thermal evaporation,[42] and sputter coating.[43] However, these methods suffer from relatively poor size and dispersion control of anchored metal particles. Therefore, an

Received: March 15, 2013
Accepted: May 29, 2013
Published: May 29, 2013

   dx.doi.org/10.1021/am401622w | ACS Appl. Mater. Interfaces 2013, 5, 5639−5647

Scheme 1. Schematic Representation of the Experimental Setup for the Doping of Pd Nanoparticles onto ZTC Using $scCO_2$ as a Solvent and $Pd(hfa)_2$ as the Pd Precursor

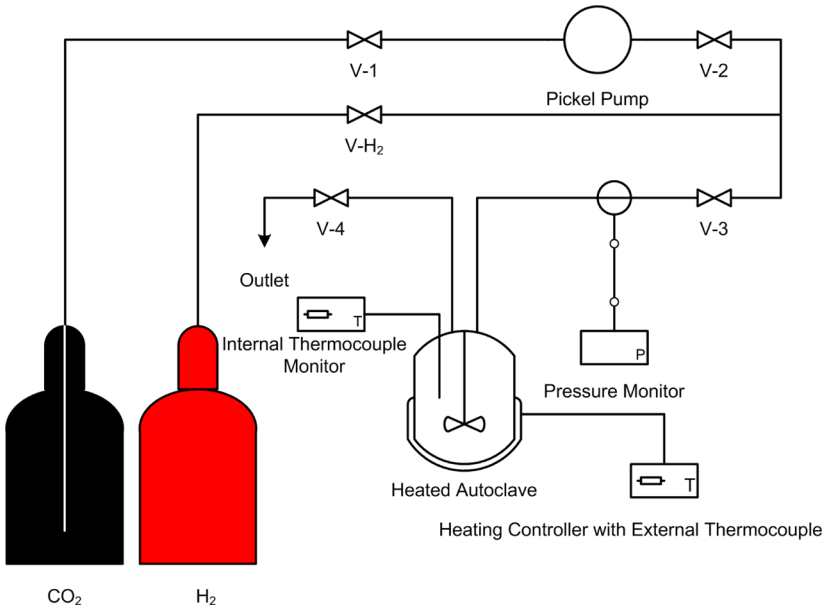

effective preparation procedure that enhances the formation of well-dispersed metal nanoparticles is highly sought after and remains an important area of research. The limitations of conventional metal implantation techniques may be overcome by using supercritical carbon dioxide ($scCO_2$) as anchoring media. $scCO_2$ is an excellent choice as reaction medium as it is easily attained due to a relatively low critical point (31.1 °C and 73.8 bar). Indeed the readily accessible conditions of $scCO_2$ coupled with it is abundance, low cost, nonflammability, and nontoxicity make it attractive as a green media/solvent in current and emerging chemical processes.[44−47] Recently $scCO_2$ has been used as solvent for depositing Pd nanoparticles onto carbon nanotubes and graphene.[46,47] In general the use of $scCO_2$ allows the deposition of well-dispersed metal nanoparticles. The size of metal particles varies between 3 and 40 nm.[46,47] It is of interest to investigate the efficiency of $scCO_2$ as media for the deposition of metal nanoparticles of a particular size in high surface area microporous carbons.

Here, we explore the possibility of improving the hydrogen uptake of zeolite templated carbons (ZTCs) by $scCO_2$ mediated incorporation of metal nanoparticles. It is believed that the presence of metals can enhance hydrogen adsorption on carbons due to overlap of the potential fields generated at the carbon pore walls and the increased polarizability of the adsorbent surface due to the presence of metal particles. Supercritical fluid (SCF) mediated metal incorporation may offer advantages arising from the liquid-like densities and gas-like properties of SCFs.[48,49] Moreover, SCF carriers possess zero surface tension, which may facilitate effective penetration into the pore channels of the microporous ZTC materials.[48−50]

2. EXPERIMENTAL SECTION

2.1. Material Synthesis. Zeolite templated carbons were obtained using zeolite Y as the hard template and acetonitrile as the carbon precursor via chemical vapor deposition as follows. An amount of 0.5 g of Zeolite Y on an alumina boat was placed in a flow-through tube furnace, which was then heated to 800 °C at a ramp rate of 5 °C/min under argon flow. Once the temperature reached 800 °C, a flow of Ar saturated with acetonitrile as the carbon precursor was passed through the furnace for 3 h followed by heat treatment at 900 °C for 3 h under a flow of Ar only. The resulting zeolite/carbon composite was allowed to cool to room temperature under Ar flow and then washed with 10% hydrofluoric acid (HF) for 24 h. The resulting carbon was filtered and washed with distilled water and was then further refluxed in hydrochloric acid at 60 °C for 6 h to ensure complete removal of the zeolite framework and finally washed with distilled water and air-dried at 120 °C. The sample was designated as ZTC8. To introduce Pd nanoparticles into the ZTC we used a procedure similar to that of Wai and co-workers.[51] The ZTC (20 mg) was mixed with the palladium hexafluoroacetylacetonoate ($Pd(hfa)_2$) precursor and loaded into a glass vial. The Pd loading (in wt %) in the mixture was varied between 0.2% and 2.0%. The mixture was then transferred into a high-pressure stainless steel autoclave (ca. 10 mL volume, 12 mm OD) as illustrated in Scheme 1. Following sample loading, valve V-2 was closed, while the rest were opened. The autoclave was purged with hydrogen gas (80 psi) at 40 °C for 30 min to expel any air. Valves V-H_2 and V-4 were then closed, and simultaneously valve V-2 was opened to charge the reactor with condensed CO_2 to a total pressure of 1160 psi, which was then left for 30 min to allow the Pd complex to penetrate the carbon framework. The temperature was increased to 80 °C (heating time of ca. 7 min) with the pressure reaching a maximum of ca. 1600 psi. The reaction vessel was then maintained at 80 °C for 10 min to allow $Pd(hfa)_2$ reduction and therefore Pd doping to occur, after which the autoclave was allowed to cool and was then flushed with CO_2 for a further 10 min before the Pd-ZTC was recovered. The Pd-loaded ZTC8 samples were designated as ZTC8Pd-*x*, where *x* is the Pd wt %. ZTC8Pd-*x* samples were prepared where *x* = 0.2, 0.4, 0.8, and 2.0%.

2.2. Material Characterization. Powder XRD analysis was performed on a Bruker D8 Advance powder diffractometer using Cu Kα radiation (λ = 1.5406 Å) and operating at 40 kV and 40 mA, with 0.02° step size and 2 s step time. Elemental composition (Pd content) was determined via X-ray fluorescence (XRF) analysis on a Philips MiniPal PW4025 XRF instrument. Thermogravimetric analysis was performed using a TA Instruments SDT Q600 analyzer under flowing air conditions. For porosity analysis, each sample was predried in an oven and then degassed overnight at 200 °C under high vacuum. The textural properties were determined by nitrogen sorption at −196 °C using a Micromeritics ASAP 2020 volumetric sorptometer. The surface area was calculated by using the BET method applied to adsorption data in the relative pressure (P/P_o) range of 0.06−0.22. The total pore volume was determined from the amount of nitrogen adsorbed at P/P_o

= 0.99. The pore size distribution was determined by a nonlocal density functional theory (NLDFT) method using nitrogen adsorption data. Transmission electron microscopy (TEM) images were recorded on photographic films developed and fixed on a JEOL 2100 FEG-TEM microscope operated at 100 kV. The samples for TEM analysis were prepared by ultrasonic dispersion of the powder products in ethanol, which were then deposited and dried on a holey carbon film on a copper-supported grid.

2.3. Hydrogen Uptake Measurements. An intelligent gravimetric analyzer (IGA) was used to measure the hydrogen storage capacity using high purity hydrogen (99.9999%). The carbon samples were dried in an oven for 24 h at 80 °C overnight and then placed in the analysis chamber and degassed at 200 °C and 10^{-10} bar for 4−6 h. The hydrogen uptake measurements were performed in the 0−20 bar pressure range at −196 °C (liquid nitrogen bath). The hydrogen uptake data were rigorously corrected for the buoyancy of the system and the samples using appropriate carbon density and hydrogen density.[18−22] The isosteric heat of adsorption (Q_{st}, kJ/mol) was determined from hydrogen adsorption isotherms obtained at liquid nitrogen (77 K) and liquid argon (87 K) temperatures based on the Clausius−Clapeyron equation.[18−20]

3. RESULTS AND DISCUSSION

3.1. Structural Analysis of Zeolite Templated Carbon. The zeolite templated carbon (ZTC8) in this study was prepared via a method that generally yields samples with a moderate level of zeolite-like ordering.[18−20,52−57] The level of zeolite-like ordering was confirmed by powder XRD analysis (Supporting Information, Figure S1), wherein sample ZTC8 showed a weak peak at $2\theta = 6°$ which could be ascribed as being similar to the (111) planes of zeolite Y. This suggests that structural regularity similar to that of zeolite Y was replicated in the carbon but only to a limited extent since the peak at $2\theta = 6°$ had a much lower intensity compared to the zeolite template. The X-ray diffraction (XRD) pattern of ZTC8 also exhibited a very broad feature at $2\theta = 26°$ which could be ascribed to the (002) diffraction from graphitic/turbostratic carbon. The very low intensity of this peak confirmed that the ZTC8 carbon was essentially amorphous.

Sample ZTC8 exhibited a nitrogen sorption isotherm (Supporting Information, Figure S2) typical of a material that possesses micropores and small mesopores. Indeed sample ZTC8 exhibits a trimodal pore size distribution with pore maxima at ca. 0.6, 1.2, and 2.4 nm. The presence of pores in the micropore range is expected given that the wall thickness of the zeolite Y framework is ca. 1.0 nm.[58] Thus, 1.2 nm pores are most probably directly templated by the zeolite framework. The difference from the expected value of 1.0 nm could be attributed to the shrinkage of carbon during carbonization and/or incomplete filling of the voids of zeolite pores.[56−61] The largest 2.4 nm pores are clearly too large to be directly templated by the zeolite. The formation of these small mesopores may be related to the extent of infiltration of the carbon precursor into the zeolite pore channels; the degree of infiltration of a carbon precursor into the zeolite channels and/or cages is expected to greatly affect the pore structure of the resultant carbons with incomplete pore filling generating larger pores (>2 nm) than those that are directly templated (ca. 1.2 nm). Johnson and co-workers reported similar pore size distribution for templated carbons and attributed the pore systems to filled and unfilled zeolite pores during the templating process.[56] The zeolite templated carbon had surface area of 2046 m^2/g and pore volume of 1.21 cm^3/g. We note that the proportion of micropore surface area and pore volume (obtained by applying t-plot analysis to adsorption data) for ZTC8 was significantly high at 75% and 61%, respectively.

3.2. Structural and Thermal Analysis of Pd-Doped Carbons. Comparison of the ZTC8 and $Pd(hfa)_2$ mixture before and after the reaction revealed a significant change in coloration from a mix of crystalline yellow and black to uniformly black throughout the mixture. Powder XRD patterns presented in Figure 1 exhibit at least four peaks for Pd-loaded

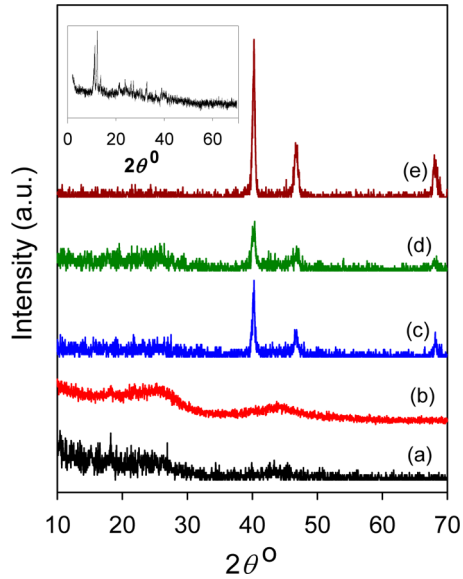

Figure 1. Powder XRD patterns of zeolite templated carbon before and after doping with Pd: (a) Pd-free ZTC8, (b) ZTC8Pd-0.2, (c) ZTC8Pd-0.4, (d) ZTC8Pd-0.8, (e) ZTC8Pd-2.0. Inset shows the XRD pattern of $Pd(hfa)_2$.

ZTC8 samples. It is worth noting that the zeolite structural ordering peak at $2\theta = 6°$ was maintained after Pd impregnation. The peaks at $2\theta = 39°$, 47°, and 68° in the pattern of the Pd-loaded samples are [111], [200], and [220] diffractions from fcc Pd crystals corresponding to *d*-spacing of 0.224, 0.193, and 0.137 nm, respectively. The powder XRD patterns for Pd-loaded samples are consistent with that reported by Howdle and co-workers in palladium−aerogel nanocomposites prepared via supercritical fluid processing.[44,45] Also, the XRD pattern of the $Pd(hfa)_2$ precursor (inset Figure 1) exhibits no peaks in the 2θ range > 20°, which further confirms that the sharp peaks in the XRD patterns of the Pd-doped samples do indeed arise from Pd nanoparticles doped onto the carbons. The amount of Pd in the doped ZTC8 samples, as determined by X-ray fluorescence (XRF) analysis, was very close to the expected values, i.e., 0.19 wt % (ZTC8Pd-0.2), 0.38 wt % (ZTC8Pd-0.4), 0.78 wt % (ZTC8Pd-0.8), and 1.92 wt % (ZTC8Pd-2.0). The use of sCO_2 as solvent, which is removed by depressurization, ensured that the ZTC carbon/Pd ratio in the reaction mixture was retained in the doped ZTCs.

Thermal analysis of the Pd precursor ($Pd(hfa)_2$), Pd-free ZTC8, and Pd-doped carbons (Supporting Information, Figure S3) was performed to ascertain thermal stability and residual mass after carbon combustion. The thermogravimetric analysis (TGA) curve of $Pd(hfa)_2$ indicates complete sublimation of the Pd precursor at 150 °C. This is attributed to the fact that $Pd(hfa)_2$ is thermally labile at low temperatures and has a low sublimation temperature.[62,63] For the carbons, some mass loss below 100 °C was observed due to removal of water or other

dx.doi.org/10.1021/am401622w | ACS Appl. Mater. Interfaces 2013, 5, 5639−5647

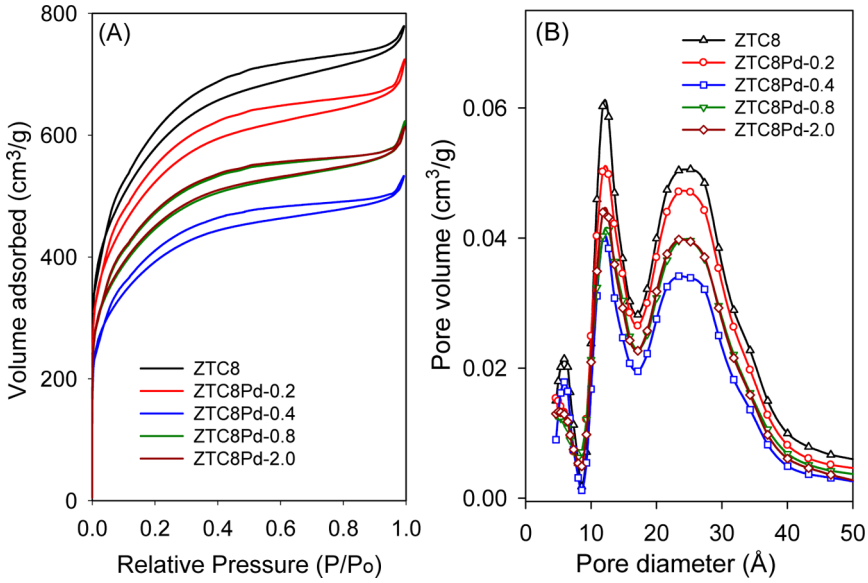

Figure 2. Nitrogen sorption isotherms (A) and corresponding pore size distribution curves (B) of Pd-free zeolite templated carbon (ZTC8) and Pd-loaded carbons.

Table 1. Textural Properties and Hydrogen Uptake Capacity of Zeolite Templated Carbon before (ZTC8) and after Pd Doping

sample	surface area (m^2/g)[a]	pore volume (cm^3/g)[b]	pore size (nm)[c]	H_2 uptake (wt %)[d]	H_2 uptake density [μmol H_2 m^{-2}]
ZTC8	2046 (1480)	1.21 (0.70)	0.6/1.2/2.4	4.9 (5.8)	12.0
ZTC8Pd-0.2	1858 (1351)	1.12 (0.63)	0.6/1.2/2.4	5.3 (7.3)	14.3
ZTC8Pd-0.4	1390 (1031)	0.82 (0.48)	0.6/1.2/2.4	5.1 (6.4)	18.3
ZTC8Pd-0.8	1597 (1187)	0.99 (0.55)	0.6/1.2/2.4	5.1 (6.6)	16.0
ZTC8Pd-2.0	1582 (1166)	0.96 (0.55)	0.6/1.2/2.4	4.7 (6.1)	14.9

[a]Values in parentheses are micropore surface area. [b]Values in parentheses are micropore volume. [c]Maxima of the pore size obtained using NLDFT analysis. [d]Hydrogen uptake capacity at 77 K and 20 bar; values in parentheses are maximum hydrogen uptake (wt %) estimated from Langmuir plots.

volatile components. While the ZTC8 carbon was completely burnt off with virtually no residual mass, the Pd-ZTC carbons left behind a residue attributed to Pd that is impregnated (i.e., occluded) onto the carbons. The fact that the Pd-doped carbons exhibited residual mass at 800 °C is further evidence for the occlusion of Pd. Furthermore, the residual mass varied according to the amount of Pd occluded in the following order: ZTC8Pd-2.0 (12%), ZTC8Pd-0.8 (10%), ZTC8Pd-0.4 (7.0%), and ZTC8Pd-0.2 (4.5%). Generally, the TGA data for the Pd-doped carbons is in good agreement with the XRD patterns; the sample with highest loading (ZTC8Pd-2.0) showed patterns with highest intensity Pd peaks. Clearly, the residual mass is rather larger than the actual amount of Pd occluded in the carbons, which raises the possibility that thermally stable Pd−C and or PdO species may be generated at high temperature during the thermal analysis.

3.3. Textural Properties and Porosity of Pd-Doped Carbons. The nitrogen sorption isotherms of the Pd-loaded samples are shown in Figure 2A. The isotherms of all the Pd-loaded samples are very similar in shape to that of the Pd-free ZTC8 sample and in all cases therefore indicate the presence of micropores and small mesopores.[64] The effect of Pd occlusion appears only to be in lowering the overall amount of nitrogen adsorbed but with no apparent effect on pore size or pore size distribution (PSD). This is confirmed by the PSD curves shown in Figure 2B; the Pd-loaded samples, similar to the Pd-free ZTC8 sample, exhibit trimodal pore size distribution centered at 0.6, 1.2, and 2.4 nm.

The textural properties of the Pd-free ZTC8 carbon and Pd-loaded samples are summarized in Table 1. As expected, the surface area and pore volume of the zeolite templated carbons reduce on Pd doping; in all cases the surface area and pore volume of the Pd-loaded samples are lower than those of the Pd-free ZTC sample. There is no clear trend between the amount of Pd and reduction in textural properties. However, for each sample, the decrease in surface area appears to be roughly similar to the reduction in pore volume. For example, the surface area decreases by 10% and 23%, whereas the pore volume reduces by 8% and 21% for samples ZTC8Pd-0.2 and ZTC8Pd-2.0, respectively. The changes in micropore surface area and micropore volume mirror those of the total surface area and pore volume. The proportion of micropore surface area (ca. 73%) and micropore volume (ca. 57%) remains unchanged after Pd doping and is unaffected by the amount of Pd doping.

3.4. Electron Microscopy Analysis of Pd-Free and Pd-Doped Carbons. The TEM images in Figure 3 for sample ZTC8 are consistent with the XRD data in showing only low levels of zeolite-like ordering. There are clearly observable void spaces (Figure 3) indicative of incomplete filling of the zeolite template pores in a manner similar to that observed by Johnson and co-workers on the effect of micropore topology on the structure and properties of zeolite polymer replicas.[56] The TEM images are also in agreement with XRD patterns that there is minimal graphitization for the ZTC8 sample.

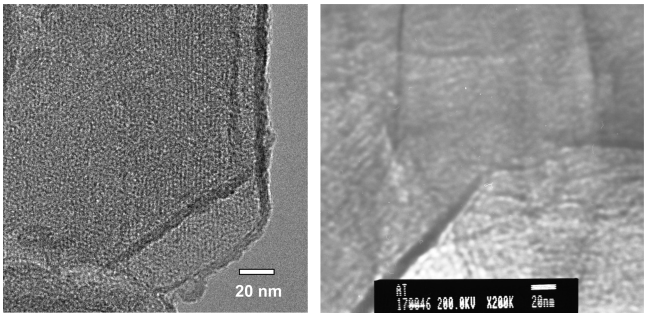

Figure 3. TEM images of zeolite templated carbon ZTC8.

The TEM image for sample ZTC8Pd-0.2 (Supporting Information, Figure S4) hardly showed any Pd particles. This indicates that at 0.2 wt % the amount of added Pd was too low to allow any significant deposition of Pd nanoparticles that are large enough to be observed under our TEM analysis conditions. Nevertheless, this sample does contain some Pd as indicated by the residual mass in the TGA data (Supporting Information, Figure S3). For sample ZTC8Pd-0.4 with 0.4 wt % Pd, we observed (Figure 4) some Pd nanoparticles of size 2−3 nm with no evidence of large Pd particles that may be located on the surface of the carbon particles. The Pd particles appear to be located within the pore channels. For sample ZTC8Pd-0.8 with 0.8 wt %, the Pd particles are easily observed as shown in Figure 4 and appear in general to be well distributed throughout the carbon particles. The size of the Pd nanoparticles is rather larger (3−5 nm) than for sample ZTC8Pd-0.4. To confirm the effect of Pd content on particle size, we prepared a sample with 4 wt % Pd, and the TEM images (Supporting Information, Figure S5) indicated spherical Pd nanoparticles of size up to 15 nm, which is similar to the report of Wai and co-workers who, using $scCO_2$, decorated multi-walled carbon nanotubes with Pd particles of 5−10 nm.[51] Selected area electron diffraction (SAED) pattern of the Pd nanoparticles (Supporting Information, Figure S5) shows concentric rings with no clear spots, indicative of Pd nanoparticles comprised of agglomerated fine crystallites.

3.5. Hydrogen Uptake. The hydrogen storage capacity of the carbons is summarized in Table 1, and the corresponding hydrogen uptake isotherms are shown in Figure 5. The hydrogen uptake isotherms show that the adsorption branch for all the samples matches the desorption branch with no hysteresis suggestive that the hydrogen sorption is fully reversible. In addition, the isotherms exhibit no saturation in the 0−20 bar pressure range indicative of the possibility of higher hydrogen uptake if the pressure is increased beyond 20 bar. A total hydrogen uptake of 4.9% (at 20 bar and 77K) for the Pd-free ZTC8 carbon, that has a surface area of 2046 m^2/g, is expected based on the known performance of zeolite templated carbons.[18−22,52−55] This hydrogen uptake is rather higher than that which would be predicted based on Chahine rule of 1 wt % uptake per 500 m^2/g of surface area.[4,65] An estimated maximum hydrogen uptake capacity of 5.8 wt % (Table 1) was computed by fitting the experimental data using the Langmuir model.[18−20,66] The data obtained for the Pd-free carbon are therefore in good agreement with previous reports on zeolite templated carbons and more generally with the

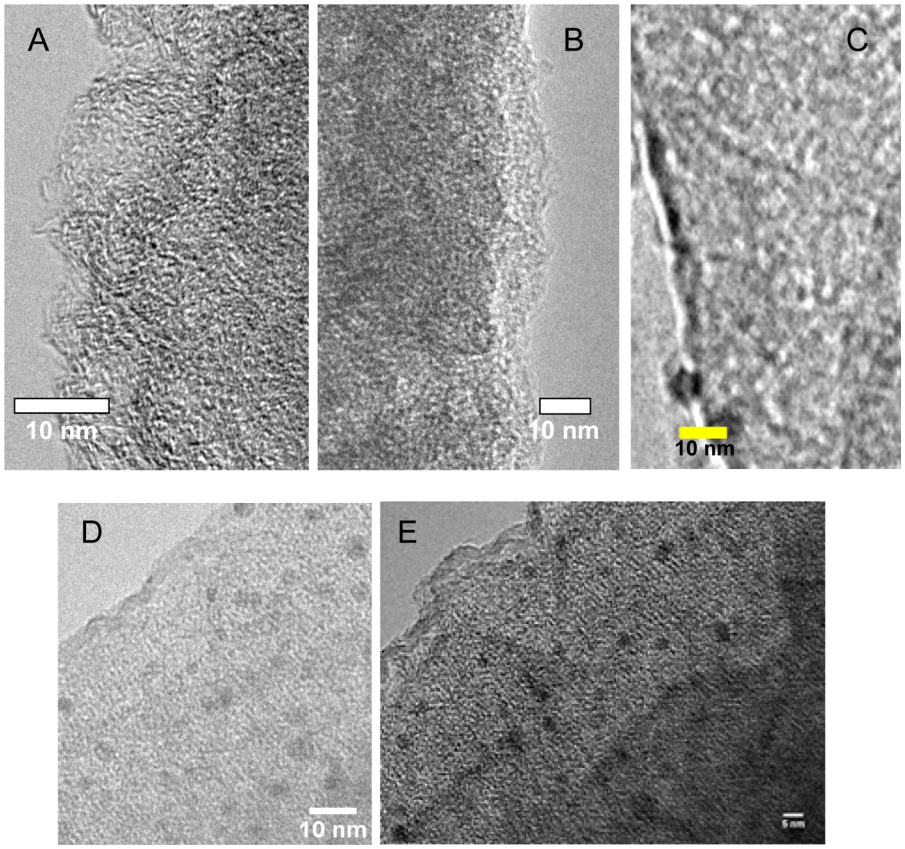

Figure 4. TEM images of ZTC8Pd-0.4 with 0.4% Pd loading (A, B, and C) and ZTC8Pd-0.8 with 0.8% Pd loading (D and E). The scale bar in E is 5 nm.

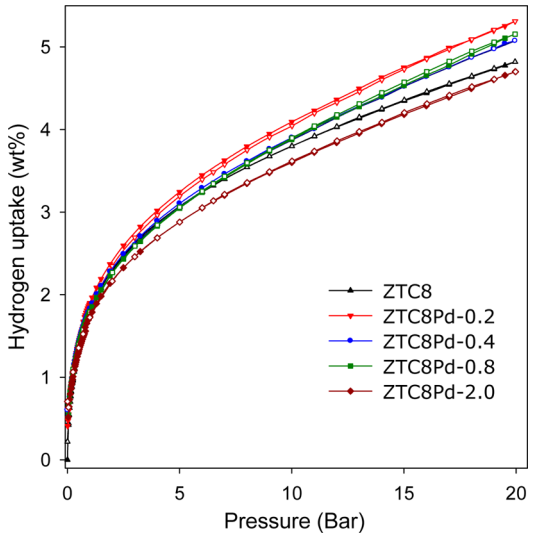

Figure 5. Total hydrogen uptake isotherms of Pd-free (ZTC8) and Pd-loaded carbons.

known relationship between hydrogen uptake and the surface area of porous materials.[18−20,67,68] It is thus surprising that despite the decrease in surface area after Pd-doping the hydrogen uptake of Pd-ZTC samples remains unchanged or in fact increases; the total hydrogen uptake of Pd-doped carbons varies between 4.7 and 5.3 wt % compared to 4.9 wt % for the parent ZTC. We note that a similar trend was observed for the excess hydrogen uptake (Supporting Information, Figure S6 and Supporting Table S1) wherein higher excess uptake is observed for the Pd-ZTC despite the decrease in surface area. Furthermore, in all cases the maximum hydrogen uptake (Table 1) is higher for Pd-ZTC than for the parent ZTC8 sample, i.e., 6.1−7.3 wt % for the doped Pd-ZTCs compared to 5.8 wt % for the bare ZTC8 sample. The hydrogen uptake data for each sample were highly reproducible with minimal variation or error; the setup of our hydrogen storage measurement regime ensures that repeat runs return virtually similar uptake data (Supporting Information, Figure S7).[13,18−20] Thus, the error in the hydrogen uptake data (at 77 K and 20 bar) given in Table 1 are very small as to be negligible (i.e., < 1% of reported values, which is typically ±0.05 wt %) and far lower than the variations between the samples. This means that the differences observed in hydrogen uptake before and after doping indicate real variation among the carbons and may not be considered as being within experimental error.

Previous studies on hydrogen storage at 77 K for metal-doped carbons have always found that metal doping decreases the surface area and thus consequently lowers the hydrogen uptake.[69,70] It is, however, worth noting that such previous studies have generally involved doping of much larger amounts of metal (typically 5 wt % and above).[69,70] This differs from the present study where the metal doping was limited to a maximum of 2 wt % and in the range 0.2−2 wt %. It is also the case that previous studies have used conventional metal doping methods (e.g., wet impregnation) wherein the distribution of metal nanoparticles is less uniform as opposed to the present study where the use of $scCO_2$ enables good metal dispersion as indicated by the TEM images in Figure 4. Previous studies have also encountered fairly large metal nanoparticles as opposed to the present study where the low Pd content (i.e., a maximum of 2 wt % Pd) ensured that the Pd particles were no larger than 5 nm and were typically in the range 2−5 nm as shown by the TEM images in Figure 4.

Many studies have claimed that the hydrogen storage capacity of carbons at ambient temperature may be improved via the so-called spillover mechanism wherein it is postulated that the increase in uptake is due to dissociative chemisorption of hydrogen on metal nanoparticles and subsequent migration of hydrogen atoms onto adjacent carbon surfaces.[71−75] While the validity of the mechanism is still under debate,[30] we note that such a process has also been claimed to occur at 77 K under certain conditions[76] and thus may explain the improved hydrogen storage of Pd-doped ZTCs, despite lowering of surface area. While most studies report that metal doping reduces the hydrogen uptake of porous materials at 77 K, some studies have shown improvement even in the face of a reduction in surface area.[76] A closer analysis of the various studies reveals that metal doping causes reduction in hydrogen storage when large amounts of metal (>5 wt %) are added.[69] On the other hand, if small amounts (≤3 wt %) are incorporated then improvements in hydrogen uptake can be observed at 77 K; for example, Cheon and co-workers observed a 43% increase in hydrogen uptake for Pd-doped MOFs that contained 3 wt % Pd despite a 40% decrease in surface area.[76] The improvement in hydrogen storage capacity was attributed to the efficiency of the small (ca. 3 nm) Pd nanoparticles in the spillover process. Clearly, larger metal particles appear to be less efficient in the spillover process and thus do not offer improvement in hydrogen uptake that can compensate for the decrease in surface area.[69,70]

We assessed the hydrogen storage density of the carbons before and after doping as summarized in Table 1. Figure 6

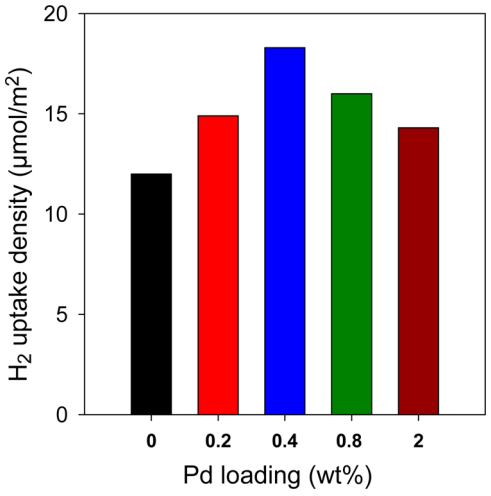

Figure 6. Hydrogen uptake density of Pd-free and Pd-loaded zeolite template carbons.

shows hydrogen uptake normalized per unit surface area (i.e., hydrogen uptake density in μmol H_2/m^2). In general the Pd-doped carbons showed higher hydrogen uptake capacity and density compared to the original Pd-free carbon. The uptake density (μmol H_2/m^2) increases from 12.0 for ZTC8 up to 18.3 for ZTC8Pd-0.4 and in all cases remains higher for the Pd-doped samples; the increase in uptake density over Pd-free carbon is up to 52%. A similar trend was observed for excess hydrogen storage density (Supporting Information, Table S1) where the improvement was up to 58%. We note that the trends in the hydrogen storage density of the carbons before

and after doping are reliable as they were calculated using hydrogen uptake isotherms which were highly repeatable (Supporting Information, Figure S7). Furthermore, to ascertain that the increase in hydrogen uptake density after Pd-doping arises from the presence of Pd and is not simply due to a decrease in surface area, we compared density of the present Pd-ZTC with ZTCs of similar surface area and pore volume (Supporting Information, Table S2).[55] The hydrogen uptake density (of ZTCs with surface area similar to the present Pd-ZTCs) varies between 9 and 13 μmol H_2/m^2 and is thus much lower than that of the Pd-ZTC samples described here. We can therefore rule out the possibility that the high uptake density of the present Pd-ZTC is simply due to a decrease in surface area. We also compared the uptake density of the present $scCO_2$ processed Pd-ZTCs with Pt-ZTC samples prepared using Pt-exchanged zeolite Y as template and Pt-ZTC samples wherein the Pt was introduced via incipient wetness (Supporting Information, Table S3).[54] The hydrogen uptake density of the Pt-ZTCs prepared via ion exchange or wet impregnation is in the range 7.6−11.6 μmol H_2/m^2 compared to 14.3−18.3 μmol H_2/m^2 for the present $scCO_2$ processed Pd-ZTC. The much higher uptake density of the $scCO_2$ processed Pd-ZTCs in this work emphasizes the advantageous role played by the use of $scCO_2$ as doping media and the effect of optimized metal content and particle size.

It is interesting to note that ZTC8Pd-0.2 gave the highest hydrogen uptake of 5.3 wt % but did not show the highest uptake density. This highlights the importance of achieving a compromise between the optimum incorporation of Pd and retention of high surface area. It thus appears that the best balance is achieved for sample ZTC8Pd-0.4, wherein the positive effect on hydrogen storage of the optimum amount of Pd taken up is sufficient to more than compensate for the decrease in surface area. The Pd particle size is, therefore, optimally small for ZTC8Pd-0.4 and thereafter grows at higher Pd content which may explain the maxima observed. The sample with 0.4 wt % Pd appears to suffer the greatest decrease in textural properties since the Pd particles are small enough to be incorporated mainly within the pore channels (Figure 4) wherein the metal particles more significantly decrease the surface area and pore volume. For samples with Pd loading of 0.8 and 2 wt %, the Pd particle size is larger, and thus some of the metal particles are not occluded within the pore channels, which rather limits the deleterious effect of the Pd on the textural properties. Overall, the hydrogen uptake data for the present Pd-loaded ZTCs show a trend similar to that observed by Yang et al. who found the order of hydrogen uptake in Ru-doped templated carbon to be 6% Ru > 8% Ru > 3% Ru.[71] This was ascribed to both reduced surface area in the case of the highest loading and a lower amount of Ru metal in the case of the lowest loading.[71] The effect of metal particle size on the hydrogen spillover effect and the beneficial effect of small particles have previously been observed.[77,78] Also, there are studies that clearly show the effect of particle size on spillover at cryogenic conditions, where either the Pd metal particle size (i.e., 3 nm)[76] or amount of Pd (i.e., 1 wt %)[79] is similar to the present work. The microscopic picture that emerges from our data is that: (i) low amounts of Pd are beneficial, (ii) small particle size is beneficial, (iii) particle size and amount of Pd are optimized for sample with 0.4 wt % Pd, thus the greatest spillover is observed, and (iv) all of the above are made possible via choice of SCFs as doping media, which allows high dispersion of Pd nanoparticles.

To further probe the influence of Pd on the hydrogen uptake, we calculated the hydrogen adsorption energy, the so-called isosteric heat of adsorption (Q_{st}). The Q_{st} was calculated using hydrogen adsorption isotherms measured at 87 and 77 K (Supporting Information, Figure S8). The adsorption branch of the hydrogen uptake isotherms was used to determine isosteric heat of adsorption based on the Clausius−Clapeyron equation. A plot of the isosteric heat of adsorption as a function of hydrogen uptake is shown in Figure 7. As expected the heat of

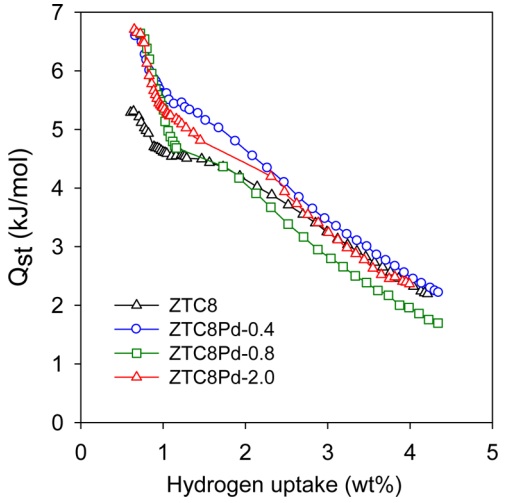

Figure 7. Isosteric heat of adsorption (Q_{st}) as a function of hydrogen uptake for Pd-free (ZTC8) and Pd-loaded zeolite templated carbons.

adsorption decreases at higher hydrogen uptake.[18−20,25,72,73] The initial Q_{st} for the Pd-free ZTC8 sample is 5.3 kJ/mol. This value is typical for porous carbons such as activated carbons (4−6.5 kJ/mol)[73−75] but lower than that of zeolite template carbons that possess narrower pore size distribution (8−10 kJ/mol).[18−20,53] We have previously demonstrated that the Q_{st} of zeolite template carbons can be significantly influenced by pore size and pore size distribution with narrower pores (0.6−0.8 nm) favoring higher Q_{st} values.[18−20,53] The initial Q_{st} for the Pd-doped carbons is ca. 6.7 kJ/mol and is in all cases higher than that of the Pd-free sample (5.3 kJ/mol). The amount of Pd (in the range 0.4−2 wt %) does not appear to have any influence on the initial Q_{st} values. The higher Q_{st} values for Pd-doped carbons are indicative of greater hydrogen−substrate interaction. The increase in Q_{st} may be attributed to the so-called "spillover" effect whereby hydrogen molecules dissociate to atomic hydrogen on a metal catalyst and migrate from the metal to the surface of carbonaceous material.[31] Similar trends have been reported by Lueking and Yang in which enhancement of hydrogen storage properties was established via hydrogen spillover onto metal particles supported on carbon nanotubes.[80,81] Given that the pore size of the Pd-free and Pd-doped carbons is similar, the higher Q_{st} for the latter can only be attributed to the presence of Pd. This implies that the higher uptake density observed for the Pd-doped carbons is likely due to a combination of higher Q_{st} and the spillover process.

4. CONCLUSIONS

Supercritical carbon dioxide has been used as solvent for the deposition of well-dispersed Pd nanoparticles onto a zeolite templated carbon (ZTC). The supercritical fluid (SCF) mediated Pd incorporation enabled the deposition of 0.2−2.0

wt % of well-dispersed Pd nanoparticles onto ZTC. While the surface area and pore volume of the ZTC decreased on Pd doping, there was no change in the pore size or pore size distribution of the carbons. Crucially, we observed that Pd incorporation enhances hydrogen uptake presumably via the so-called spillover process. Although the surface area and pore volume decreased significantly (by up to 30%) on Pd incorporation, the hydrogen uptake was largely unchanged or increased. This in effect translated to a much higher hydrogen storage density for the Pd-doped carbons. Thus, while the ZTC (with surface area of 2046 m^2/g) had a total hydrogen storage capacity (at 77 K and 20 bar) of 4.9 wt %, the Pd-ZTCs had uptake of 4.7−5.3 wt % despite surface area in the range 1390−1858 m^2/g. The Pd-ZTCs thus exhibit enhanced hydrogen storage density (14.3−18.3 μmol H_2/m^2), which is much higher than that of Pd-free ZTC (12.0 μmol H_2/m^2). A similar trend was observed in the excess hydrogen storage and excess hydrogen storage density. The hydrogen storage density goes through maximum at 0.4 wt % Pd loading. The enhancement in hydrogen uptake was made possible by deposition of only small amounts (up to 2 wt %) of Pd, which were highly dispersed in the form of small (2−5 nm) nanoparticles. The hydrogen isosteric heat of adsorption (Q_{st}) was found to be higher for the Pd-doped carbons (6.7 kJ/mol) compared to the parent ZTC (5.3 kJ/mol). Our findings provide insight into the process of optimizing the balance between metal loading/particle size and surface area to achieve the best metal/carbon composite for enhanced hydrogen uptake.

■ ASSOCIATED CONTENT

Supporting Information

Three additional tables; excess hydrogen storage data for the zeolite templated carbon (ZTC8) and Pd-doped carbons Pd-ZTC8, and published hydrogen uptake data for metal doped zeolite templated carbons prepared via liquid impregnation or ion exchange, and eight additional figures; Powder XRD, nitrogen sorption isotherm and pore size distribution curves of zeolite template (CBV100) and zeolite templated carbon (ZTC8), TGA data of Pd precursor ($Pd(hfa)_2$), zeolite templated carbon (ZTC8) and Pd-doped carbons Pd-ZTC8, TEM images of Pd-ZTC8 carbons with 0.2 wt % and 4 wt % Pd loading, excess hydrogen storage data for the zeolite templated carbon (ZTC8) and Pd-doped carbons Pd-ZTC8, cycles of hydrogen sorption profiles for a variety zeolite templated carbons and hydrogen uptake isotherms of Pd-free and Pd-doped ZTCs obtained at 77 K and 87 K. This material is available free of charge via the Internet at http://pubs.acs.org.

■ AUTHOR INFORMATION

Corresponding Author

*E-mail: r.mokaya@nottingham.ac.uk.

Notes

The authors declare no competing financial interest.

■ ACKNOWLEDGMENTS

We thank Prof. Andrei Khlobystov for assistance with TEM measurements and the Nottingham Nanoscience and Nanotechnology Centre (NNNC) for access to the electron microscope. We thank Prof. Martyn Poliakoff for assistance with SCF experiments.

■ REFERENCES

(1) van den Bergm, A. W. C; Arean, C. O. *Chem. Commun.* **2008**, 668−681.
(2) Thomas, K. M. *Catal. Today* **2007**, *120*, 389−398.
(3) Ahmadpour, A.; Do, D. D. *Carbon* **1996**, *34*, 471−479.
(4) Sevilla, M.; Alam, N.; Mokaya, R. *J. Phys. Chem. C* **2010**, *114*, 11314−11319.
(5) Sevilla, M.; Fuertes, A. B.; Mokaya, R. *Energy Environ. Sci.* **2011**, *4*, 1400−1410.
(6) Sevilla, M.; Foulston, R.; Mokaya, R. *Energy Environ. Sci.* **2010**, *3*, 223−227.
(7) Sevilla, M.; Mokaya, R. *J. Mater. Chem.* **2011**, *21*, 4727−4732.
(8) Sevilla, M.; Fuertes, A. B.; Mokaya. *Int. J. Hydrogen Energy* **2011**, *36*, 15658−15663.
(9) Ryoo, R.; Joo, S. H.; Jun, S. *J. Phys. Chem. B* **1999**, *103*, 7743−7746.
(10) Sakintuna, B.; Yürüm, Y. *Ind. Eng. Chem. Res.* **2005**, *44*, 2893−2902.
(11) Kyotani, T. *Bull. Chem. Soc. Jpn.* **2006**, *79*, 1322−1337.
(12) Xia, Y.; Mokaya, R. *J. Phys. Chem. C* **2007**, *111*, 10035−10039.
(13) Xia, Y.; Walker, G. S.; Grant, D. M.; Mokaya, R. *J. Am. Chem. Soc.* **2009**, *131*, 16493−16499.
(14) Xia, Y.; Mokaya, R.; Grant, D. M.; Walker, G. S. *Carbon* **2011**, *49*, 844−853.
(15) Almasoudi, A.; Mokaya, R. *J. Mater. Chem.* **2012**, *22*, 146−152.
(16) Xia, Y.; Mokaya, R. *Chem. Vap. Deposition* **2010**, *16*, 322−328.
(17) Xia, Y.; Yang, Z.; Mokaya, R. *Nanoscale* **2010**, *2*, 639−659.
(18) Yang, Z.; Xia, Y.; Mokaya, R. *J. Am. Chem. Soc.* **2007**, *129*, 1673−1679.
(19) Yang, Z. X.; Xia, Y. D.; Sun, X. Z.; Mokaya, R. *J. Phys. Chem. B* **2006**, *110*, 18424−18431.
(20) Masika, E.; Mokaya, R. *J. Phys. Chem. C* **2012**, *116*, 25734−25740.
(21) Kowalczyk, P.; Gauden, P. A; Terzyk, A. P.; Bhatia, S. K. *Langmuir* **2007**, *23*, 3666−3672.
(22) Wang, Q. Y.; Johnson, J. K. *J. Chem. Phys.* **1999**, *110*, 577−586.
(23) Texier-Mandoki, N.; Dentzer, J.; Piquero, T.; Saadallah, S.; David, P.; Vix-Guterl, C. *Carbon* **2004**, *42*, 2744−2747.
(24) Cabria, I.; Lopez, M. J.; Alonso, J. A. *Carbon* **2007**, *45*, 2649−2658.
(25) Yushin, G.; Dash, R.; Jagiello, J.; Fischer, J. E.; Gogotsi, Y. *Adv. Funct. Mater.* **2006**, *16*, 2288−2293.
(26) Vix-Guterl, C.; Frackowiak, E.; Jurewicz, K.; Friebe, M.; Parmentier, J.; Beguin, F. *Carbon* **2005**, *43*, 1293−1302.
(27) Gogotsi, Y.; Portet, C.; Osswald, S.; Simmons, J. M.; Yildirim, T.; Laudisio, G.; Fischer, J. E. *Int. J. Hydrogen Energy* **2009**, *34*, 6314−6319.
(28) Gogotsi, Y.; Dash, R. K.; Yushin, G.; Yildirim, T.; Laudisio, G.; Fischer, J. E. *J. Am. Chem. Soc.* **2005**, *127*, 16006−16007.
(29) Zlotea, C.; Cuevas, F.; Paul-Boncour, V. R.; Leroy, E.; Dibandjo, P.; Gadiou, R.; Vix-Guterl, C.; Latroche, M. *J. Am. Chem. Soc.* **2010**, *132*, 7720−7729.
(30) Giasafaki, D.; Bourlinos, A.; Charalambopoulou, G.; Stubos, A.; Steriotis, T. *Microporous Mesoporous Mater.* **2012**, *154*, 74−81.
(31) Chen, C.-H.; Huang, C.-C. *Microporous Mesoporous Mater.* **2008**, *109*, 549−559.
(32) Chen, C.-Y.; Chang, J.-K.; Tsai, W.-T.; Hung, C.-H. *J. Mater. Chem.* **2011**, *21*, 19063−19068.
(33) Ye, X. R.; Lin, Y.; Wai, C. M. *Chem. Commun.* **2003**, 642−643.
(34) Zacharia, R.; Kim, K. Y.; Fazle Kibria, A. K. M.; Nahm, K. S. *Chem. Phys. Lett.* **2005**, *412*, 369−375.
(35) Stadie, N. P.; Purewal, J. J.; Ahn, C. C.; Fultz, B. *Langmuir* **2010**, *26*, 15481−15485.
(36) Campesi, R.; Cuevas, F.; Leroy, E.; Hirscher, M.; Gadiou, R.; Vix-Guterl, C.; Latroche, M. *Microporous Mesoporous Mater.* **2009**, *117*, 511−514.
(37) Levy, R. B.; Boudart, M. *J. Catal.* **1974**, *32*, 304−314.
(38) Teichner, S. J. *Appl. Catal.* **1990**, *62*, 1−10.

(39) Bhat, V. V.; Contescu, C. I.; Gallego, N. C. *Nanotechnology* **2009**, *20*, 204011.
(40) Prins, R. *Chem. Rev.* **2012**, *112*, 2714−2738.
(41) Figueiredo, J. L.; Pereira, M. F. R.; Serp, P.; Kalck, P.; Samant, P. V.; Fernandes, J. B. *Carbon* **2006**, *44*, 2516−2522.
(42) Bittencourt, C.; Felten, A.; Ghijsen, J.; Pireaux, J. J.; Drube, W.; Erni, R.; Van Tendeloo, G. *Chem. Phys. Lett.* **2007**, *436*, 368−372.
(43) Zhang, Y.; Dai, H. *Appl. Phys. Lett.* **2000**, *77*, 3015−3017.
(44) Morley, K. S.; Licence, P.; Marr, P. C.; Hyde, J. R.; Brown, P. D.; Mokaya, R.; Xia, Y.; Howdle, S. M. *J. Mater. Chem.* **2004**, *14*, 1212−1217.
(45) Darr, J. A.; Poliakoff, M. *Chem. Rev.* **1999**, *99*, 495−542.
(46) Wu, C. H.; Wang, C. H.; Lee, C. H. M. T.; Chang, J. K. *J. Mater. Chem.* **2012**, *22*, 21466−21471.
(47) Chen, C. H.; Chang, J. K.; Tsai, J. K.; Hung, C. H. *J. Mater. Chem.* **2011**, *21*, 19063−19068.
(48) Cooper, A. I. *Adv. Mater.* **2003**, *15*, 1049−1059.
(49) Zhang, Y.; Erkey, C. *J. Supercrit. Fluids* **2006**, *38*, 252−267.
(50) Sakintuna, B.; Yurum, Y. *Ind. Eng. Chem. Res.* **2005**, *44*, 2893−2902.
(51) Ye, X. R.; Lin, Y.; Wang, C.; Engelhard, M. H.; Wang, Y.; Wai, C. M. *J. Mater. Chem.* **2004**, *14*, 908−913.
(52) Pacula, A.; Mokaya, R. *J. Phys. Chem. C* **2008**, *112*, 2764−2769.
(53) Alam, N.; Mokaya, R. *Energy Environ. Sci.* **2010**, *3*, 1773−1781.
(54) Alam, N.; Mokaya, R. *Microporous Mesoporous Mater.* **2011**, *142*, 716−724.
(55) Alam, N.; Mokaya, R. *Microporous Mesoporous Mater.* **2011**, *144*, 140−147.
(56) Johnson, S. A.; Brigham, E. S.; Ollivier, P. J.; Mallouk, T. E. *Chem. Mater.* **1997**, *9*, 2448−2458.
(57) Kyotani, T.; Nagai, T.; Inoue, S.; Tomita, A. *Chem. Mater.* **1997**, *9*, 609−615.
(58) Ma, Z.; Kyotani, T.; Tomita, A. *Carbon* **2002**, *40*, 2367−2374.
(59) Rodriguez-Mirasol, J.; Cordero, T.; Radovic, L. R.; Rodriguez, J. J. *Chem. Mater.* **1998**, *10*, 550−558.
(60) Guan, C.; Wang, K.; Yang, C.; Zhao, X. S. *Microporous Mesoporous Mater.* **2009**, *118*, 503−507.
(61) Su, F.; Zhao, X. S.; Lv, L.; Zhou, Z. *Carbon* **2004**, *42*, 2821−2831.
(62) Bhaskaran, V.; Hampden-Smith, M. J.; Kodas, T. T. *Chem. Vap. Deposition* **1997**, *3*, 85−90.
(63) Hasell, T.; Wood, C. D.; Clowes, R.; Jones, J. T. A.; Khimyak, Y. Z.; Adams, D. J.; Cooper, A. I. *Chem. Mater.* **2010**, *22*, 557−564.
(64) Sing, K. S. W.; Everett, D. H.; Haul, R. A. W.; Moscou, L.; Pierotti, R. A.; Rouquerol, J.; Siemieniewska, T. *Pure Appl. Chem.* **1985**, *57*, 603−619.
(65) Sevilla, M.; Fuertes, A. B; Mokaya, R. *Energy Environ. Sci.* **2011**, *4*, 2930−2936.
(66) Zheng, Z.; Gao, Q.; Jiang, J. *Carbon* **2010**, *48*, 2968−2973.
(67) Wong-Foy, A. G.; Matzger, A. J.; Yaghi, O. M. *J. Am. Chem. Soc.* **2006**, *128*, 3494−3495.
(68) McKeown, N. B.; Gahnem, B.; Msayib, K. J.; Budd, P. M.C.; Tattershall, E.; Mahmood, K.; Tan, S.; Book, D.; Langmi, H. W.; Walton, A. *Angew. Chem., Int. Ed.* **2006**, *45*, 1804−1807.
(69) Zlotea, C.; Campesi, R.; Cuevas, F.; Leroy, E.; Dibandjo, P.; Volkringer, C.; Loiseau, T.; Ferey, G.; Latroche, M. *J. Am. Chem. Soc.* **2010**, *132*, 2991−2997.
(70) Sculley, J.; Yuan, D.; Zhou, H. C. *Energy Environ. Sci.* **2011**, *4*, 2721−2735.
(71) Wang, L.; Yang, R. T. *J. Phys. Chem. C* **2008**, *112*, 12486−12494.
(72) Srinivas, G.; Zhu, Y.; Piner, R.; Skipper, N.; Ellerby, M.; Ruoff, R. *Carbon* **2010**, *48*, 630−635.
(73) Bénard, P.; Chahine, R. *Langmuir* **2001**, *17*, 1950−1955.
(74) Zhou, L.; Zhou, Y.; Sun, Y. *Int. J. Hydrogen Energy* **2004**, *29*, 475−479.
(75) Zhao, X. B.; Xiao, B.; Fletcher, A. J.; Thomas, K. M. *J. Phys. Chem. B* **2005**, *109*, 8880−8888.
(76) Cheon, Y. E.; Paik, S. M. *Angew. Chem., Int. Ed.* **2009**, *48*, 2899−2903.
(77) Wang, L.; Stuckert, N. R.; Chen, H.; Yang, R. T. *J. Phys. Chem. C* **2011**, *115*, 4793−4799.
(78) Stuckert, N. R.; Wang, L.; Yang, R. T. *Langmuir* **2010**, *26*, 11963−11971.
(79) Sabo, M.; Henschel, A.; Fröde, H.; Klemm, E.; Kaskel, S. *J. Mater. Chem.* **2007**, *17*, 3827−3832.
(80) Lueking, A. D.; Yang, R. T. *Appl. Catal., A* **2004**, *265*, 259−268.
(81) Lueking, A. D.; Yang, R. T. *J. Catal.* **2002**, *206*, 165−168.